Fission gas release from irradiated UO_2 fuel : Development of new mechanistic code MFPR and applications.

R.Dubourg[1*], M.S. Veshchunov[2], G.Nicaise[1], V.E. Shestak[2] , V.Tarasov[2]

1 : Institut de Radioprotection et de Sûreté Nucléaire,BP3 13115 St Paul lez-durance CEDEX (France)

2 : Nuclear Safety Institute of the Russian Academy of Sciences(IBRAE) Moscow (Russia)

corresponding author :** roland.dubourg@irsn.fr **0033442256513

ABSTRACT

MFPR code is a mechanistic code developed in collaboration between IBRAE (Russia) and IRSN (France). It describes both intra and inter-granular fission gas behaviour in different realistic situations such as in-reactor irradiation regime or LOCA transients or high temperature annealing modes. It includes improvements in the classical re-solution effects, from irradiation and from thermal effects. A new formulation of the grain growth model is proposed. The main specificity concerns the strong interaction between intra-granular gas and point or extended defects. The vacancy model included in the code allows self-consistent calculation of bubble nucleation factor, realistic description of grain bubble relaxation and implementation of model for enhanced bubble mobility in the vacancy field created at the end of annealing regime. The dislocation creep model, implemented for annealing regime, explains the observed burst release during high temperature ramps.

Examples are given on ADAGIO, FLASH and VERCORS experiments, giving satisfying results. Further improvements are proposed concerning the grain growth model, dislocation model which might be extended to irradiation regime and the thermal resolution model.

Keywords: Fission gas release, MFPR, grain boundaries inventory, LOCA, VERCORS.

1. INTRODUCTION

Any realistic description of fission gas release and fuel swelling as a function of fuel-fabrication variables and a wide range of reactor operating conditions must include many mechanisms.

In this field, the code MFPR (Module for Fission Product Release) is being developed for mechanistic description of gas behaviour in several conditions development. It includes refinement of the existing mechanistic codes FASTGRASS [1] and VICTORIA [2]. As such, it constitutes a tool for interpretation of many experiments or for reliable prediction of gas behaviour in specific conditions.

In this paper, the main characteristics and current status of the MFPR code, description of the new models, are presented regarding fission gas behaviour. This fission gas modelling is applied to three different situations : first, to irradiation regime during reactor operations conditions in the case of high burn-up fuel; then, to transient LOCA type conditions; finally, to out of pile annealing conditions at high temperature, up to 2573K.

2. PHYSICAL PROCESSES AND MODELS FOR FISSION GASES IN MFPR

In MFPR, the process of the FP release from solid fuel is divided into two consequent stages :

- Intra-granular gas transport from the bulk to the grain boundary then transfer in the inter-granular bubbles,
- accumulation of fission gases in the inter-granular bubbles, and release to the open porosity through the system of bubbles on the grain boundaries and the net channels and tunnels. The model ignores the delay related to the gas transfer both through the net channels and through the open porosity.

In the grain, the main phenomena included in the code are :

·FP atom generation, diffusion to grain boundaries and capture by grain bubbles (or re-solution from these bubbles).
·Bubble nucleation, growth, diffusion and biased migration in temperature and vacancy gradients to grain boundaries.
·Bubbles coalescence and sweeping by grain boundaries (recrystallisation) and by dislocations (creep).
·Vacancy field evolution and interactions with gas atoms and bubbles.

Inter-granular bubbles are classified into three groups : bubbles on the grain faces (GF), on the grain edges (GE) and in the grain corners (GC). The GF bubble growth progresses up to the grain surface saturation, when interlinkage of the GF bubble and formation of grain face channels to the grain edges and corners occur. Growth of the GE and GC bubbles leads to their interconnection by tunnels and formation of open porosity.

2.1 Intra-granular fission gases transport (bimodal representation)

For gas atoms the transport equation in the grain takes the general form (in spherical geometry for a grain, considered in the code as a tetrakaidecahedron[1]) :

$$\frac{\partial C_g}{\partial t} = \nabla \left(D_g \nabla C_g \right) - \omega_{bmg} \left(v_g \right) C_g - F_{g \to b} + \omega_{fis} \qquad (1)$$

C_g is the gas atoms concentration, D_g is the gas diffusion coefficient expressed from Killeen-Turnbull formulation [3] and v_g is the biased mobility of atoms.
The first term describes random atoms transport, the second term concerns biased migration (grain boundary sweeping associated with grain growth), the fourth term represents creation by fission. The third one represents atoms interaction with bubbles including bubble nucleation (ω_{nuc}), capture of atoms by bubbles (ω_{cap}, including thermal re-solution of atoms, for C_{eq} see eq 7) and re-solution of atoms from bubbles by irradiation effects (ω_{rsi}).

$$F_{g \to b} = \omega_{nuc} C_g^2 + \omega_{cap} \left(C_g - C_{eq} \right) C_b - \omega_{rsi} \varphi(N_b) Y_b \qquad (2)$$

[1] with, when the grain is surrounded by its neighbours, 7 faces, 12 edges, and 6 corners.

Strongly associated with the above formulations for atoms in grain, the following equations are proposed for atoms in bubbles (with Y_b their volume concentration).

$$\frac{\partial Y_b}{\partial t} = \nabla\left(D_b \nabla Y_b\right) - \omega_{bmg}(v_b) Y_b + F_{g\to b}, \quad Y_b = N_b C_b \qquad (3)$$

The mean number of atoms in a bubble evolution is given by

$$\frac{\partial N_b}{\partial t} = \omega_{cls} Y_b - \omega_{nuc} \frac{C_g^2}{2C_b} + \omega_{cap}\left(C_g - C_g^{eq}\right) - \omega_{rsi} N_b \varphi(N_b) \qquad (4)$$

The first term of equation (4) deals with bubble coalescence associated to bubble diffusivity which is expressed from classical effects of surface diffusion, plastic deformation and vaporisation-condensation [1] or from Mikhlin's formulation [4].

From classical mechanistic codes [1,2], MFPR is rather specific on the following points.

2.1.1 Re-solution effects (irradiation +thermal)

According to [5], re-solution of gas atoms by irradiation occurs from a thin periphery layer ($\lambda \approx$ 1–1.5 nm) of bubbles. However, the ejection of a gas atom into surrounding matrix does not automatically result in its re-solution, because within the re-solution layer $\delta \sim$ 1 nm, atoms would tend to return back to the bubble. This gives :

$$dN_b/dt = 4\pi D c_g R_b - b' N_b , \qquad (5)$$

with the renormalised expression for the re-solution probability b' (from b_0 that of pure Nelson's model) :

$$b' \approx b_0[\lambda/(\lambda + R_b)]\cdot[\delta/(\delta + R_b)]. \qquad (6)$$

In the case of thermal re-solution, the kinetic equation for the number N_b of gas atoms in a bubble with the radius R_b under annealing conditions in the Van-der-Waals approximation, takes the form :

$$\frac{dN_b}{dt} = 4\pi D_g R_g [c_g - c_g^{eq}], \qquad (7)$$

where $c_g^{eq} = PK_s\varphi(P,T)$, and $\varphi(P,T) = \exp(B_{Xe}P/kT)$, is the function accounting for the gas phase non-ideality in the Van-der-Waals approximation (k the Boltzman constant), P is the pressure within the bubbles, T is the temperature, B_{Xe} is the Van-der-Waals parameter for *Xe*, and $K_s(T)$ is the *Xe* solubility in UO_2 (K_s is supposed to be of Arrhenius type temperature dependent with adjusted parameters).

2.1.2 Point defects (vacancies and interstitials) effects

The characteristics of grain bubbles are strongly dependent on the concentration of point defects [6]. The bubble nucleation factor is equal to the vacancy concentration which in addition determines bubble relaxation. Also, in some annealing conditions, the vacancy gradient inside the grain makes additional possibility for increased bubble mobility [7].

In MFPR, the general expression for vacancy evolution is :

$$\frac{\partial c_v}{\partial t} = D_v \Delta c_v - 4\pi D_v R_b C_b \left(c_v - c_v^{bs}\right) - \left[D_v Z_v \rho_d \left(c_v - c_v^{eq}\right) + \alpha D_i c_i c_v\right] + K \qquad (8)$$

with c_v and c_i number of vacancies and interstitials per uranium atom, D_v and D_i correspondingly the vacancy and interstitial diffusion coefficients, α the recombination constant, $K = F z_s \Omega$ is the atomic displacement rate where F is the fission rate, Ω the vacancy molar volume and z_s is the damage formation in the fission track volume. The dislocation sink strength constant Z_v for vacancies is of the order of unity.

In Eq.(8), the thermal equilibrium vacancy concentration, c_v^{eq}, is approximated by Arrhenius correlation. The second term in the right hand side of Eq.(8) describes a mechanism of the vacancy sink into bubbles that is connected intimately with the bubble relaxation. The boundary concentration of vacancies at the bubble surface, c_v^{bs}, is given by :

$$c_v^{bs} = c_v^{eq} \exp\left(-\Omega \delta P / kT\right). \qquad (9)$$

It depends on difference between the actual and equilibrium bubble gas pressures, δP, defined as :

$$\delta P = P - P_h - \frac{2\gamma}{R_b}, \qquad P = \frac{N_b kT}{\left(V_b - B_{Xe} N_b\right)} \qquad (10)$$

where P_h is the external hydrostatic pressure, γ is the effective surface tension for UO_2, P is the gas pressure within a bubble given by the Van-der-Waals equation of state, V_b is the bubble volume.

Deviation from equilibrium gas pressures together with the non-equilibrium vacancy and interstitial concentrations determines the rate of the bubble volume relaxation:

$$\frac{dV_b}{dt} = 4\pi R_b \left(D_v \left(c_v - c_v^{bs}\right) - D_i c_i\right) \qquad (11).$$

In the case of steady–state irradiation conditions, bubble relaxation can be regarded as a fast process, and the bubble volume, V_b, can be approximated using the equilibrium equation according to which $\delta P = 0$ and $c_v^{bs} = c_v^{eq}$.

In annealing conditions, the vacancy diffusivity is related to the equilibrium uranium self-diffusion coefficient, D_U^{eq}, by

$$c_v^{eq} D_v = D_U^{eq}.$$

D_U^{eq} and D_v are approximated by Arrhenius correlations [8] and the relaxation rate is given by eq 11 but with neglecting effects of interstitials (D_iC_i).

2.1.3 Extended defects (dislocations) effects

Sweeping of bubbles by moving dislocations may induce gas release at high temperature.

A model is implemented into MFPR (for post–irradiation conditions) with the main following simplifications.

- Dislocation loops formation and growth are not taken into consideration during the annealing stage (segments of dislocation lines only).
- Once attached to dislocation segment, gas particle does not leave it inside the fuel grain.

Dislocation creep mechanism is described in terms of two variables : the dislocation density, ρ_d, and the atoms-on-dislocations density, Y_d. The fluxes $F_{g\to d}$ and $F_{b\to d}$ describing the

attachment of gas atoms and bubbles to dislocations are added to corresponding transport equations for C_g and C_b (Eqs 1 and 3). Variables, ρ_d and Y_d, satisfy following equations :

$$\frac{\partial Y_d}{\partial t} = F_{g\to d} + F_{b\to d} - \left[\omega_{bmg}(v_d) Y_d + 2\nabla(D_v \nabla c_v)\right] \qquad (12)$$

$$\frac{\partial \rho_d}{\partial t} = -\omega_{bmg}(v_d)\,\rho_d \qquad (13)$$

where the dislocation velocity is defined as:

$$v_d = v_d^0 \varphi_d\left(R_b^{(d)}, N_b^{(d)}\right)\left(1 - \frac{c_v}{c_v^{eq}}\right), \quad v_d^0 = \frac{2\pi D_u}{B\ln(L/R_d)} \text{ the intrinsic mobility ,}$$

φ_d being the pinning factor (by attached bubbles) :

$$\varphi_d\left(R_b^{(d)}, N_b^{(d)}, Y_d, \rho_d\right) = \frac{1}{1 + \dfrac{B^2 v_d^{(0)} Y_d}{\rho_d N_b^{(d)} D_b^{(d)}}} \qquad (14)$$

Here B is the Burger's vector length (lattice parameter), L characterises mean distance between dislocations, R_d is the dislocation core radius.

If the number of atoms captured by dislocations is sufficiently small to satisfy the inequality

$$2R_b^{(d)} Y_d / N_b^{(d)} < \rho_d ,$$

the characteristics, $R_b^{(d)}$ and $N_b^{(d)}$ (size and mean number of atoms in bubbles), of bubbles captured by dislocations are equal to the corresponding bulk values (R_b and N_b).

After complete coverage of dislocations, the condition $c_b^{(d)} 2R_b = 1$ is applied giving rapid coalescence of bubbles attached to dislocations and strong pinning of dislocations. This means that after rapid growth of bubble radius within one order of magnitude the dislocation velocity will practically turn to zero, i.e. dislocations will be pinned by attached bubbles. At this time, the main source of vacancies is grain boundary and strong vacancy gradient could enhance grain bubble diffusivity from the simple relation (Evan's mechanism [7]) :

$$v_b^{vac}(r) = 2D_v \frac{\partial c_v}{\partial r} \qquad (15)$$

2.1.4 Grain growth

A new approach was developed from [9]. In presence of inter-granular bubbles, the grain boundary velocity, v_{gb}, is written as:

$$v_{gb} = \frac{d}{dt} d_{gr} = v_{gb}^0 \varphi_{gb} \qquad (16)$$

where v_{gb}^0 is the base velocity , φ_{gb} is the retarding factor, d_{gr} the grain diameter.

In the general case of different types of intergranular bubbles (face '*f*', edge '*e*', and corner '*c*') the retarding factor can be written as:

$$\varphi = \left(1 + \frac{81 v_{gb}^{(0)} kT R_{gr}^2}{16\xi\gamma_{gb}}\left(\frac{n_f}{D_b^f} + \frac{n_e}{D_b^e} + \frac{n_c}{D_b^c}\right)\right)^{-1} .$$

The base grain boundary velocity is approximated by the Arrhenius type correlation:

$$v_{gb}^{(0)} = v_0 \left(\frac{R_0}{R_{gr}} \right)^n \exp\left(-E_{gb}/kT\right) \qquad (17)$$

where $R_0 = 10\mu m$ is the scale factor, v_0, n, and E_{gb} are fitted parameters on Bourgeois tests [10].

2.2 Inter-granular fission gases transport

2.2.1 Intergranular swelling model

Any gas transferred to grain boundary as atoms or bubbles belongs to inter-granular porosities, first to face bubbles population. Coalescence of face bubbles due to their random migration is considered as the main mechanism of grain face bubbles relaxation [11,12], on the base of the general theory of grain face bubbles migration and coalescence [13].
The general equation for the evolution of face bubbles concentration is written in the form:

$$\frac{dX_f}{dt} = \omega_{nuc} X_g^2 - \omega_{cls} X_f^2 \qquad (18)$$

where ω_{nuc} is frequency of bubble nucleation, ω_{cls} is frequency of coalescence of bubbles, X_g is surface concentration of atoms on grain faces.
Coalescence frequency of bubbles randomly moving on a surface can be represented by :

$$\omega_{cls} = \frac{8\pi D_b}{\ln\left(\frac{D_b}{2R_f^2}\tau_0\right)} \approx 8\pi\alpha D_b \qquad (19)$$

where τ_0 is the characteristic time of two-fold increase of the mean bubble radius R_f. D_b is represented in a form depending on the dominating microscopic mechanism of bubble migration, fitted on experimental data [9].

2.2.2 Modes for FP Release by Bubble Interlinkage

The equations governing the gas transport from the system of inter-granular to the open porosity are based on a percolation type approach [14]. In the case of grain face bubbles, the rate equation takes the form

$$\frac{d}{dt} Y_f = F_{gas}\,\theta_f, \qquad \theta_f \equiv \theta(A^* - A_f) \qquad (21)$$

where $\theta(x)$ is a Heaviside step function (= 0 for x <0, =1 in other cases), A_f is the projected area coverage of the grain face by the GF bubbles and the constant A^* is set equal to 0.5 [2], A_f is the gas flux to the grain boundary. The critical area coverage of the grain face determines the onset of formation of the interconnected channels from GF bubbles to the grain edges.

The rate equations for the concentration of a gas component in the GE and GC bubbles are of the form

$$\frac{d}{dt}Y_e = \eta_e F_{gas}(1-\theta_f)\theta_e,$$

$$\frac{d}{dt}Y_c = \eta_c F_{gas}(1-\theta_f)\theta_e \qquad (22)$$

where (with $\eta_c = \eta_e = ½$).

$$\theta_e \equiv \theta(L^* - l_e N_{bpe}) \qquad (23)$$

L^* is given by $L^* = L_{edge} - 2R_c$, L_{edge} is the average edge length, l_e is the effective length of edge bubble, and N_{bpe} is the number of edge bubbles per grain edge. Equation 23 determines the formation of the long-range interconnection of GE and GC bubbles to the open porosity.

Finally, the gas release rate is determined by

$$\frac{d}{dt}Y_{out} = F_{gas}(1-\theta_f)(1-\theta_e) \qquad (24)$$

where Y_{out} is the concentration of the gas component released from the fuel.

2.2.3 Xe grain face diffusion transport

The current version of MFPR includes an improved model for the transport of *Xe* atoms that self-consistently takes into account the effects of atom diffusion along the grain surface and irradiation re-solution from intergranular bubbles [11, 15].

The surface diffusion model is formulated in terms of the fluxes to GF, GE and GC bubbles :

$$F_f = F_\delta - F_{f\to ec} - \omega^f_{rsi} Y_f$$

$$F_e = \eta_e F_{f\to ec} - \omega^e_{rsi} Y_e$$

$$F_c = \eta_c F_{f\to ec} - \omega^c_{rsi} Y_c .$$

F_δ describes an overall flux of xenon atoms deposited on grain boundaries :

$$F_\delta = F^{(Xe)}_{gb} + F_{rsi}$$

where $F^{(Xe)}_{gb}$ is volume density of overall flux of xenon atoms out of fuel and F_{rsi} is the sum of resolution fluxes from all extra-granular bubbles:

$$F_{rsi} = \omega^f_{rsi} Y^{(Xe)}_f + \omega^e_{rsi} Y^{(Xe)}_e + \omega^c_{rsi} Y^{(Xe)}_c$$

ω being the re-solution rates. These fluxes self-consistently determine built-up concentration barrier c_δ of the resolution layer, which reduces the diffusion flux from the grain $F^{(Xe)}_{gb}$ and determines the net flux deposited on the grain boundary $F_\delta \approx Dc_\delta/\delta$.

3. APPLICATIONS OF MFPR CODE

During its development, MFPR code was validated on many separate effect tests in steady irradiation regime [16,17,18,19,20], in transient between two irradiation regimes [21,22] or in post irradiation annealing regime [10,23,24]. This code was alto recently applied to more realistic configurations or transients regarding more macroscopic observations as will be shown in the following paragraphs.

3.1 Gas distribution during reactor operations

Specific experiments were performed by CEA in ADAGIO facility in order to quantify locally the partition of gas inventories between grain boundary and matrix after irradiation regime prior any transient or after such a transient [25].

A test involving a high burn-up fuel of about 60 GWd/tU is considered here. The results given by a fuel performance code were used for evaluation of radial variations of temperature and fission rate of the samples, needed by MFPR as boundary conditions.

Table 1 compares experimental and calculated results for inner and outer zones (derived from experimental sampling but not rim zone) of pellets from the nearly medium axial elevation of the above mentioned fuel rod. This comparison deals with relative fractions of gas released, gas in intra-granular locations (atoms or bubbles), gas in inter-granular locations.

In outer zone, the temperature lies between 1050K and 822K decreasing during reactor operations. The fission rate decreases also from $1.6.10^{19}/m^3/s$ to $7.10^{18}/m^3/s$. In inner zone temperature decreases from 1270 to 1065K and fission rate from $1.5.10^{19}/m^3/s$ to $8.810^{18}/m^3/s$. Table 1 shows very satisfying results for outer zone whereas, for inner zone, the intra-granular gas content is overestimated by the code and gas release and inter-granular content are underestimated.

Figure 1 shows the gas behaviour in inner pellet zone during reactor operations from MFPR modelling. These results were obtained considering a grain diameter of 11µm. It is shown that at the beginning of operations, the low amount of grain bubbles allows migration of gas atoms to the grain boundaries and significant increase in concentration and size of face bubbles. Nearly around 10GWd/tU the grain face coverage is reached and growth of edge and corner porosities begins. The bubble interlinkage is obtained near 20GWd/tU leading to the beginning of gas release.

In figure 2 are given the mean radius and mean concentration of grain bubbles. For inner zone the results are rather consistent with those proposed from experimental evidences at 20GWd/tU by [20] and for comparable temperature by [26]. In that way the parameters for bubble nucleation and re-solution seem convenient with perhaps a sligth underestimation of bubble size and overestimation of bubble concentration. At higher burn-up, the authors of [20] showed that a second bubble population is created, with higher size (20-100nm) and lower concentration ($10^{21}/m^3$). Very often this population is near dislocations : this is not reproduced by the code in its present state.

For inner location, increasing gas atoms diffusion coefficient increases significantly the gas release (despite increase of bubble nucleation and atoms capture by bubbles). It is possible to obtain a value very close to that experimentally derived but with higher under-estimation of inter-granular content. At these rather low temperatures the thermal part of diffusion coefficient is low but the a-thermal part could be underestimated in the code formulation.

Another more reliable explanation is linked to the well known fuel restructuring effect. Very often, in inner part of the pellets some grain growth is observed leading to the possibility of fission gases transfer due to grain shrinkage. In our case, at low temperatures, the code does not calculate any grain growth. In fact, at the beginning of reactor operations when inter-granular porosities were not significantly created, some grain growth might have occurred leading to early transfer of gases out of grain then to early release. Later, the new grain size could prevent interlinkage, giving significant inter-granular content. Thus the temperature dependence of base grain boundary velocity (see eq 17) could be reviewed.

3.2 LOCA type conditions

MFPR gas modelling in reactor operations permits to evaluate further gas behaviour and release during LOCA type transient. Such transient was reproduced in FLASH5 experiment [27] on irradiated fuel (50GWd/tU).

The global gas release was measured after the test for each nuclide. For stable gases the relative fraction was estimated at 6%. For such experimental conditions, the gas behaviour calculated by MFPR is described in figure 3 for outer radial locations in the pellet (a similar curve is obtained for inner location with low intergranular content).

The relative gas release fraction (reported to local creation) from outer location is about 9% (5% for inner location). The results obtained from MFPR calculations might be considered as satisfying because both values bracken the experimental result. The quick temperature rise induces significant increase of the size of inter-granular porosities which reach interlinkage criteria leading to creation of open porosities and gas release.

In this temperature range (and for a very quick sequence) no release can be foreseen from the grain itself. Indeed, the temperature increase gives higher atoms diffusivity which results in higher nucleation and capture by bubbles (in addition some bubble coalescence is observed). At such low temperatures there is no mechanism to explain any bubble release and the sequence is too short to allow any gas atom release by diffusion. The grain content remains the same but with a significant transfer of gases from atoms to bubbles.

3.3 High temperature annealing conditions

Such conditions are reproduced in VERCORS experiments [28] as for instance in the VERCORS 4 test for irradiated fuel (~40GWd/tU) at high temperature (1573 then 2573K).

Figure 4 gives the gas release from MFPR calculation compared to the experimental value. Note that the calculation deals with stable gases and the experimental values with short half-life gas. Figure 5 represents the calculated intra-granular gas behaviour during the experiment.
During the oxidation plateau, thermal re-solution transferred some Xe atoms from grain bubbles into the fuel matrix leading to grain bubble concentration decrease in connection with gas atoms concentration increase (see figure 6). This effect gives some few additional gas release due to atoms motion, underestimated compared to experimental values.
Then, during temperature ramp, there is a very sharp drop of this concentration mainly due to significant increase of the bubble diffusivity, accentuated in the case of the Mikhlin's formulation where the migration of bubbles is assumed to be caused by mass transport both on the bubble surface and through the matrix around the bubble [4]. This leads to bubble capture by dislocations and to grain bubble coalescence and mean grain bubble radius strong increase as explained in paragraph 2.1.3..
Just after bubble coalescence, Xe atoms capture becomes very significant and the atom concentration sharply decreased (figure 6).
The strong bubble capture by dislocation occurred after clad oxidation plateau. This is related to bubble radius increase and dislocation velocity increase. This velocity increases because the uranium self diffusivity (D_U) becomes significant at these temperatures but also and mainly because the pinning factor increases during a short time due to the high value of bubble diffusivity as expressed by Mikhlin's formulation. This is a very important point of MFPR model which implies that dislocation velocity is still significant even after important dislocation coverage.
This leads to important dislocation creeping and corresponding release of trapped Xe (atoms or bubbles). This effect is a short time process which explains the burst Xe release calculated.

After dislocation pinning (ie after 10^4s) (figure 7), the grain boundary becomes the main source of vacancies and the vacancy field becomes significant (see figure 8 between 11000 and 13000s) allowing enhanced grain bubble mobility [7] (see eq 16). The vacancy concentration is equal to thermal equilibrium value at the beginning of experiment since no point defects are created by irradiation in this case. At low temperature (300K at the beginning) vacancy diffusivity is very low which means that the vacancy concentration at the bubble surface is equal to the bulk concentration (c_{vac}). In addition it is likely that δP (eq 10) is very low and thus this bulk concentration is near the thermal equilibrium value. When temperature rises up to nearly 800K at the first temperature plateau, δP increases reducing bubble surface vacancy concentration and bulk vacancy concentration. In the "high temperature" part of the test, the vacancy concentration increases again in relation with temperature and reach the final thermal equilibrium value at the end of experiment
In the final part of the transient, some calculated gas release is due to grain growth. The calculated mean grain size increased from 15µ to 22.5µ whereas no grain growth was seen experimentally in relation with the formulation of retarding effect of inter-granular porosities.

5. CONCLUSIONS

MFPR code includes many improvements in the classical re-solution effects for both irradiation (intra and inter-granular effects with diffusion on grain boundaries) and thermal effects. Also, the

grain growth model was reviewed and new formulation proposed. The main specificity of MFPR concerns the strong interaction between intra-granular gas and point or extended defects. The vacancy model allows self-consistent calculation of bubble nucleation factor, realistic description of grain bubble relaxation and enhanced bubble mobility in the vacancy field created at the end of annealing regime. The dislocation creep model, implemented for annealing regime, explains the observed burst release during high temperature ramps.

Applied to situations like in-reactor irradiation regime or LOCA transients or high temperature annealing modes, the code gives satisfying results. It is shown that a good evaluation of gas inventory between inter and intra granular location is of prime importance for reliable evaluation of gas release in LOCA conditions.
Nevertheless, some discrepancies were highlighted and permitted to propose further improvements. Namely, reactor irradiation calculations showed that the grain growth model might be reviewed for intrinsic grain boundary mobility. Also, the dislocation model might be extended to this regime in order to self-consistently calculate the dislocation behaviour allowing rim zone formation by grain subdivision in the case of high density of dislocations and to reproduce the creation of the new high size bubble population observed at high burn-up.
In annealing regime, it was shown that the thermal resolution model might be reviewed. A very important question concerns the bubble growth mechanism above 1600K which determines further bubbles behaviour. The model describing interaction between bubbles and dislocations might be improved, (in relation with bubble diffusivity formulation).

REFERENCES

[1] J. Rest, S.A. Zawadzki, "FASTGRASS, A Mechanistic Model for the Prediction of Xe, I, Cs, Te, Ba and Sr release from Nuclear Fuel under Normal and Severe-Accident Conditions", NUREG/CR-5840 TI92 040783, 1994.

[2] T.J. Heames et al. "VICTORIA : A Mechanistic Model of Radionuclide Behavior in the Reactor Coolant System Under Severe Accident Conditions", NUREG/CR-5545 SAND90-0756 Rev 1 R3, R4, 1992.

[3] J.C.Killeen and J.A.Turnbull. "An experimental and theoretical treatment of the release of Kr from hypostoichiometric uranium dioxide", Proc. of Workshop Chemical Reactivity of Oxide Fuel and Fission Product Release, Berkeley, April 7-9, 1987.

[4] E.Ya.Mikhlin, J.Nucl.Mater., 87 (1979), p. 405

[5] R.S.Nelson. , J. Nucl. Mater. v.31 (1969), p.153-161.

[6] M.S.Veshchunov, J. Nucl.Mat. v.227 (2000), p.67–81.

[7] J.H.Evans, J. Nucl. Mater., 246 (1997) 121

[8] H.Matzke. Adv. Ceram. v.17 (1986), p.1

[9] V.D.Ozrin, V.E.Schestak, V.I.Tarasov, M.S.Veshchunov. "MFPR MODULE ver. 1.3.1. Validation Study", IBRAE Report, NSI–SARR–140–2002, November 2002

[10] L.Bourgeois, Ph.Dehaudt, C.Lemaignan, J.P.Fredesic. J. Nucl. Mater., 295 (2001) 73

[11] I. Zacharie, S. Lansiart, P. Combette, M. Trotabas, M. Coster, M. Groos, J. Nucl. Mater., 255 (1998) 85-91.

[12] A.V. Berdyshev and M.S. Veshchunov, "Modelling of grain face diffusion transport and swelling in UO_2 fuel", - Preprint IBRAE-2002-14, Moscow, 2002. [12] J.
[13] Ya.E. Geguzin and M.A. Krivoglaz, "The Movement of Microscopic Inclusions in Solid State", Metallurgiya, Moscow, 1971, (in Russian).
[14] R.J. White and M.O. Tucker, J. Nucl. Mater., 118 (1983) 1-38.
[15] M.S. Veshchunov, A.V. Berdyshev, V.I. Tarasov, Development of Fission Gas Bubble Models for UO_2 Fuel in Framework of MFPR Code,- Preprint IBRAE-2000-08, Moscow, 2000.
[16] C. Baker, J. Nucl. Mater., 71 (1977) 117.
[17] R.M Cornell J. Nucl. Mater., 38 (1971) 319
[18] J.A Turnbull J. Nucl. Mater., 38 (1971) 203
[19] H.Zimmermann, J. Nucl. Mater., 75 (1978) 154.
[20] S. Kashibe, K. Une , K.Nogita J. Nucl. Mater., 206 (1993) 22
[21] M Mogensen and C.Bagger, J. Nucl. Mater., 199 (1993) 85
[22] I.L.F.Ray, H.Thiele, Hj.Matzke, J. Nucl. Mater., 188 (1992) 90
[23] G.J.Small, AERER 12956, Harwell Laboratory, May 1988
[24] K. Une, S. Kashibe, J. Nucl. , J. Nucl. Mater., 189 (1992) 210.
[25] S.Ravel et al in "Fission Gas Behaviour in Water Reactor Fuels" Seminar proceedings Cadarache, France 26-29 September 2000 (p 347)
[26] C. Baker, J. Nucl. Mater., 66 (1977) 283
[27] M.Bruet et al "High burn up fuel behavior during a LOCA type accident : The FLASH 5 experiment". Proceedings of the IAEA Technical Comittee Meeting on "Behavior of Core Material and Fission Products Release in Accident Conditions in LWR's". Cadarache, France 16-20 March 1992.
[28] G. Ducros, P.P. Malgouyres, M. Kissane, D. Boulaud, M. Durin, Nucl. Eng . Design., 208 (2001) 191-203.

FIGURE CAPTION

Table 1: Gas location during reactor operations for inner and outer radial zones of an irradiated fuel (60MWd/tU). Comparison between experimental results and those from MFPR (1.3.1) calculations

Figure 1: Gas behaviour in inner radial zone of an irradiated fuel (60MWd/tU) given by MFPR1.3.1 calculation

Figure 2 : Grain bubble characteristics (mean radius and concentration) given by MFPR (1.3.1) calculation for inner and outer radial zones on an irradiated fuel (60MWd/tU).

Figure 3: Inter-granular gas behaviour and release calculated by MFPR(1.3.1) for outer pellet radial location in a LOCA type experiment performed on irradiated fuel (~50GWd/tU) (FLASH5 experience).

Figure 4: Comparison for gas release values in VERCORS 4 experiment between MFPR (1.3.1) calculation (for stable gases) and experimental values (for short half-life ^{135}Xe).

Figure 5: Intra-granular gas behaviour in VERCORS 4 calculated by MFPR (1.3.1)

Figure 6: Evolution of the characteristics (radius and concentration) of grain bubbles and of gas atoms concentration in grain in VERCORS 4, calculated by MFPR (1.3.1).

Figure 7: Dislocation coverage factor (in each radial mesh) in VERCORS 4, calculated by MFPR (1.3.1).

Figure 8: Evolution of the vacancy concentration in VERCORS 4 calculated by MFPR (1.3.1). This concentration is expressed relative to the thermal equilibrium value and given for each radial mesh of the grain.

	INNER ZONE			OUTER ZONE		
	Intra gas	*Inter gas*	*Released*	*Intra gas*	*Inter gas*	*Released*
MFPR / Exp	*1.15*	*0.6*	*0.6*	*1*	*1.3*	*0.5*

Table 1: Gas location during reactor operations for inner and outer radial zones of an irradiated fuel (60MWd/tU). Comparison between experimental results and those from MFPR (1.3.1) calculations

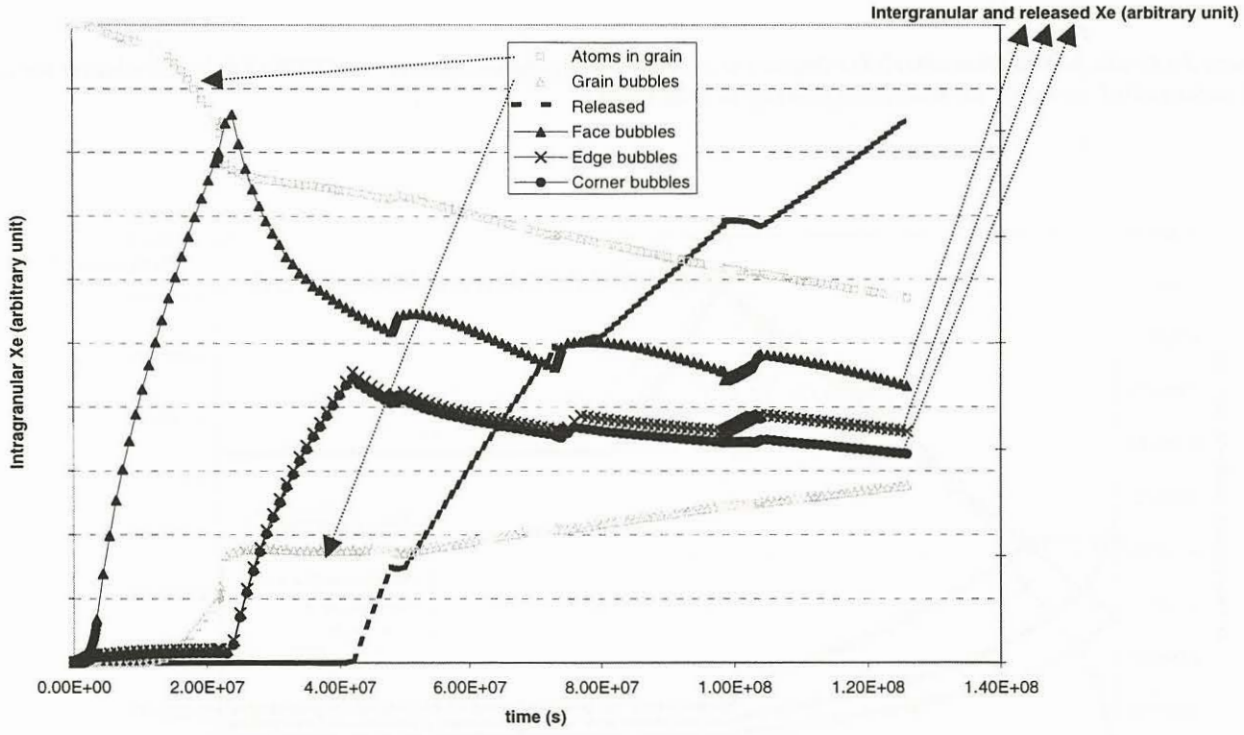

Figure 1: Gas behaviour in inner radial zone of an irradiated fuel (from 0 to 60MWd/tU) given by MFPR1.3.1

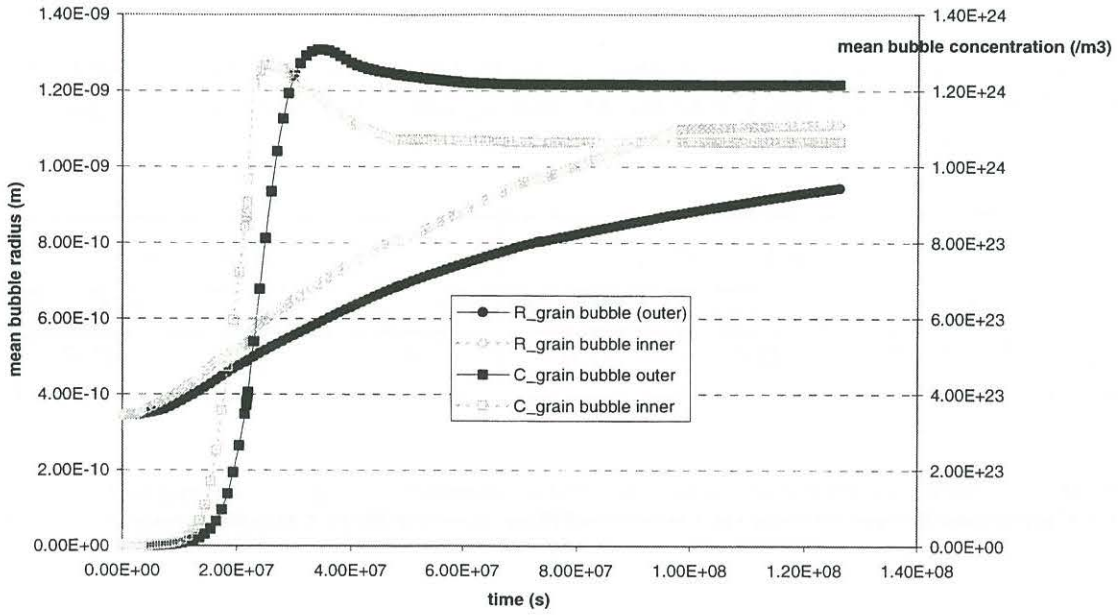

Figure 2 : Grain bubble characteristics (mean radius and concentration) given by MFPR (1.3.1) calculation for inner and outer radial zones on an irradiated fuel (up to 60MWd/tU).

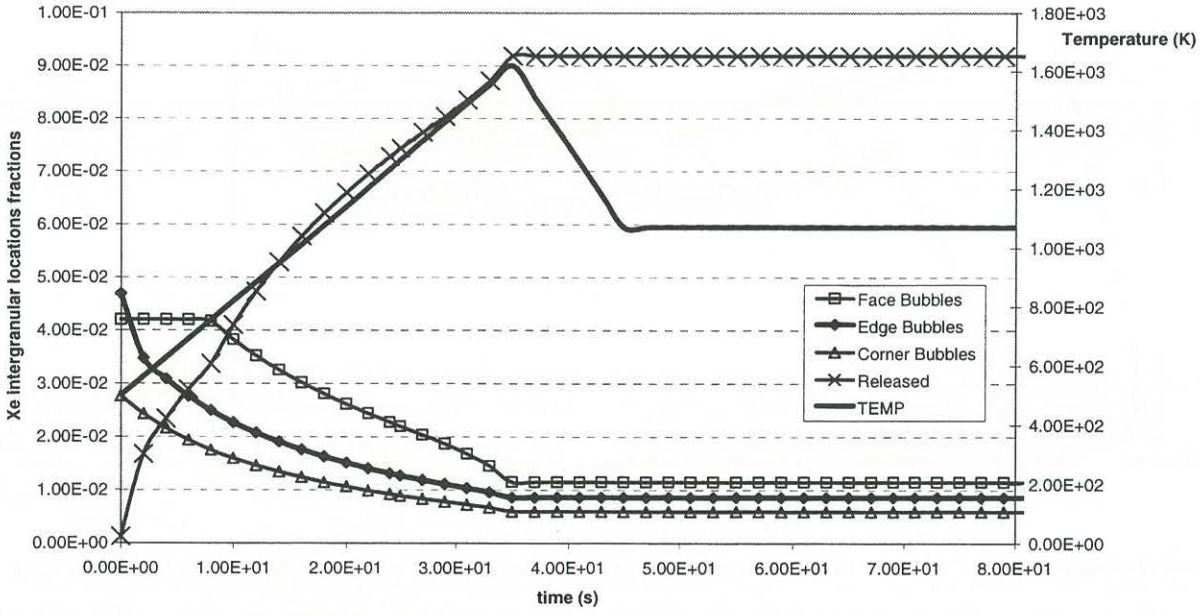

Figure 3: Inter-granular gas behaviour and release calculated by MFPR(1.3.1) for <u>outer</u> pellet radial location in a LOCA type experiment performed on irradiated fuel (~50GWd/tU) (FLASH5 experiment).

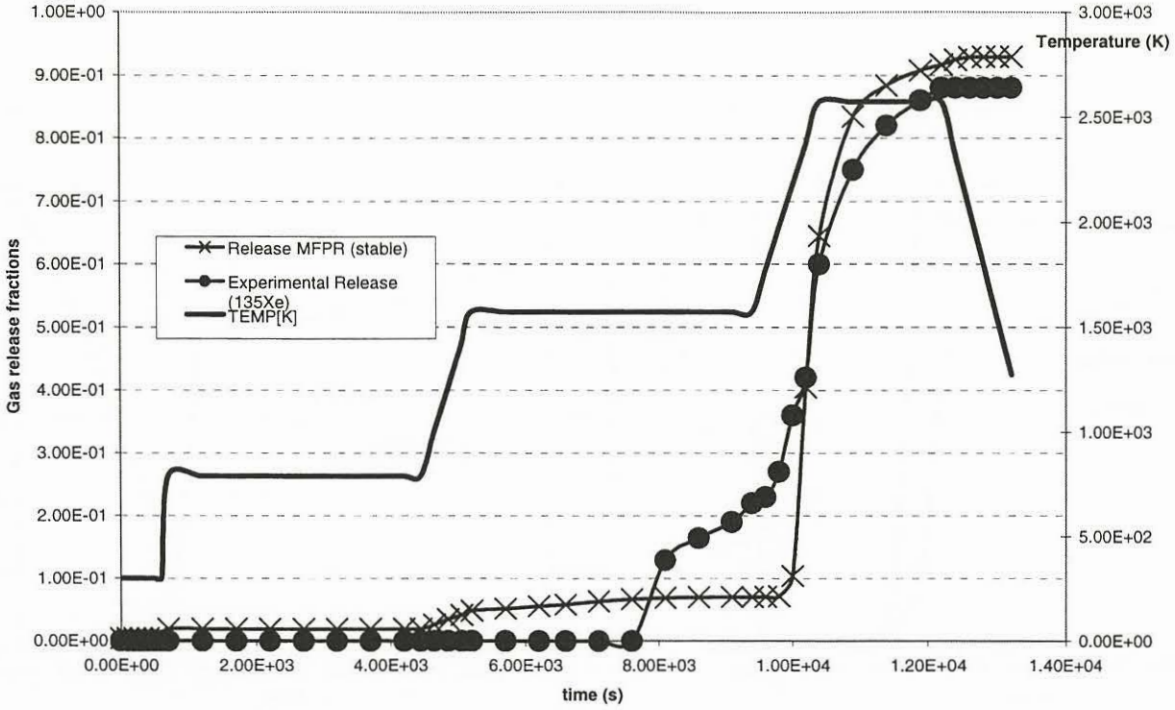

Figure 4: Comparison for gas release values in VERCORS 4 experiment between MFPR (1.3.1) calculation (for stable gases) and experimental values (for short half-life ^{135}Xe).

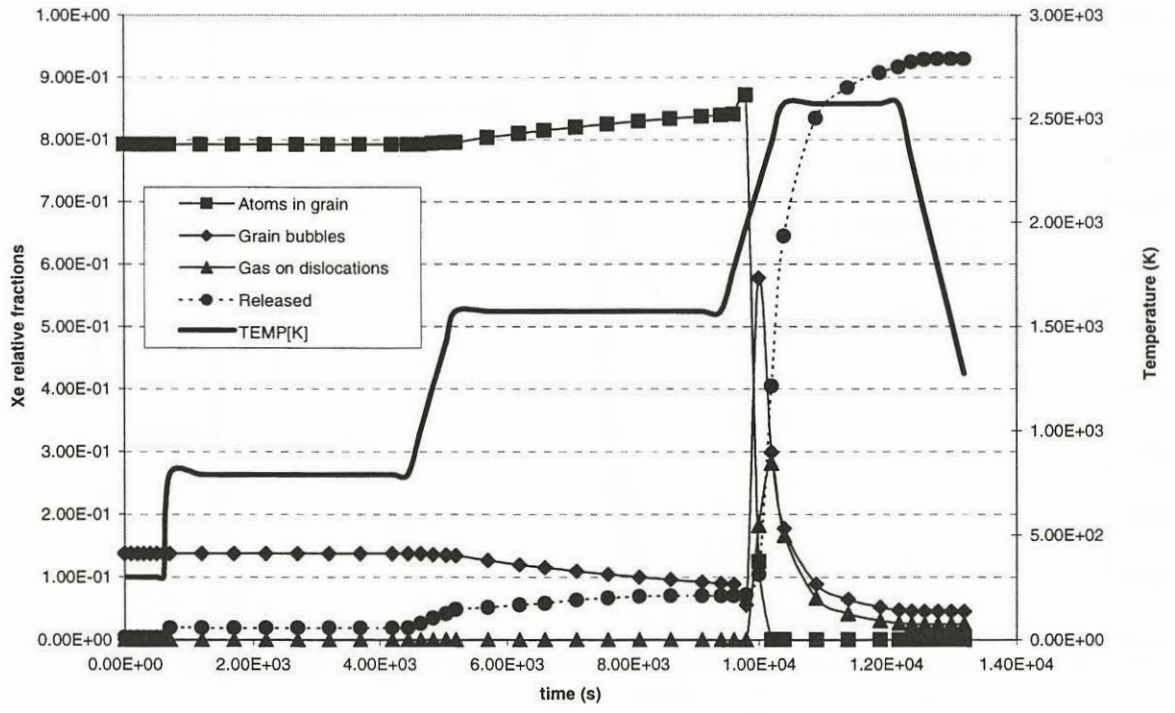

Figure 5: Intra-granular gas behaviour in VERCORS 4 calculated by MFPR (1.3.1)

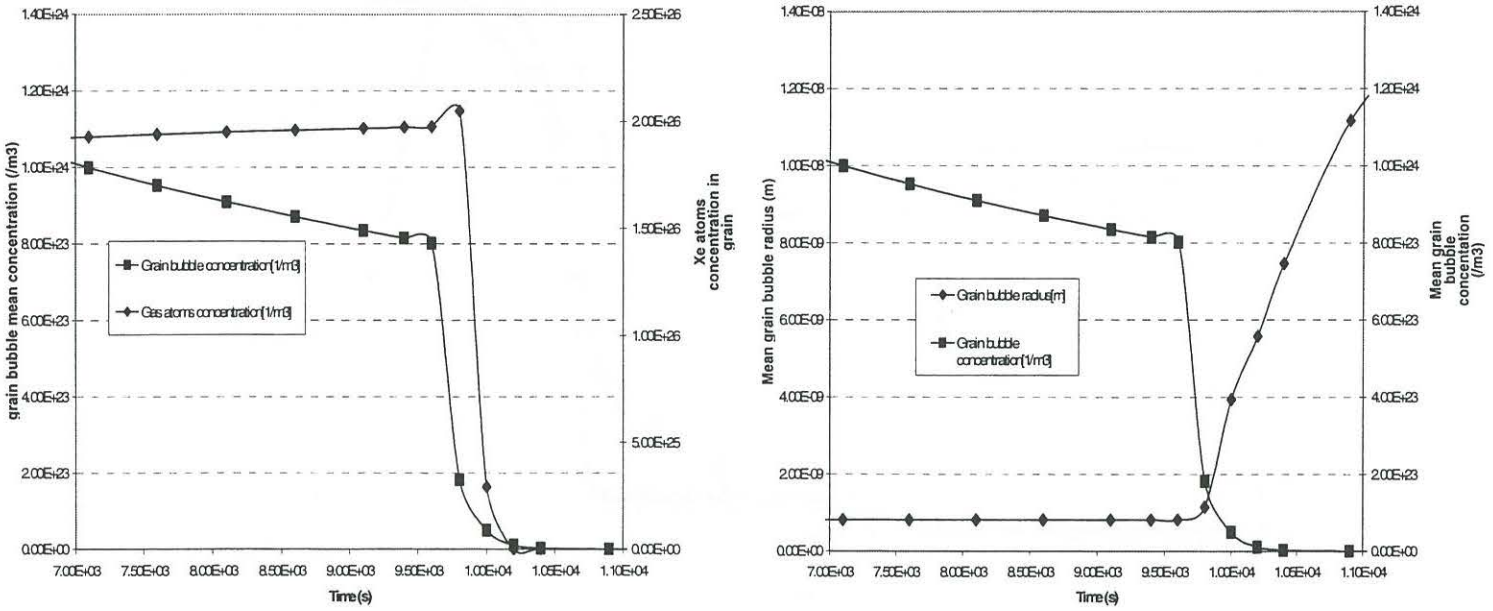

Figure 6: Evolution of the characteristics (radius and concentration) of grain bubbles and of gas atoms concentration in grain in VERCORS 4, calculated by MFPR (1.3.1).

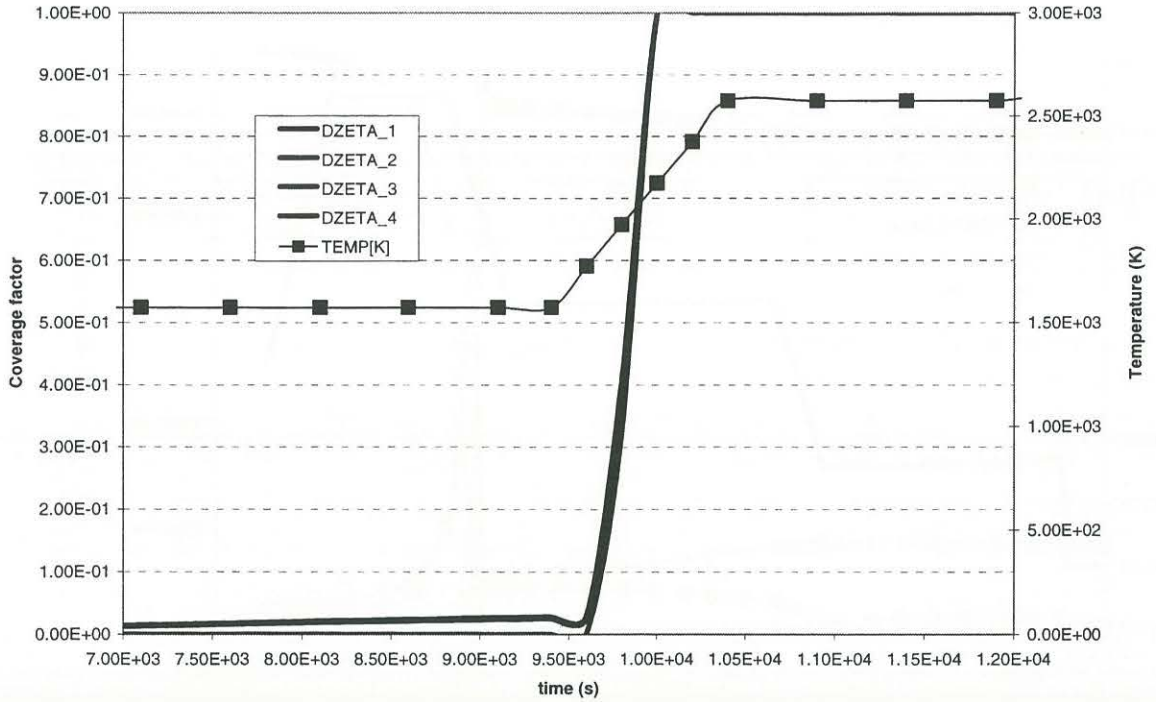

Figure 7: Dislocation coverage factor (in each radial mesh) in VERCORS 4, calculated by MFPR (1.3.1).

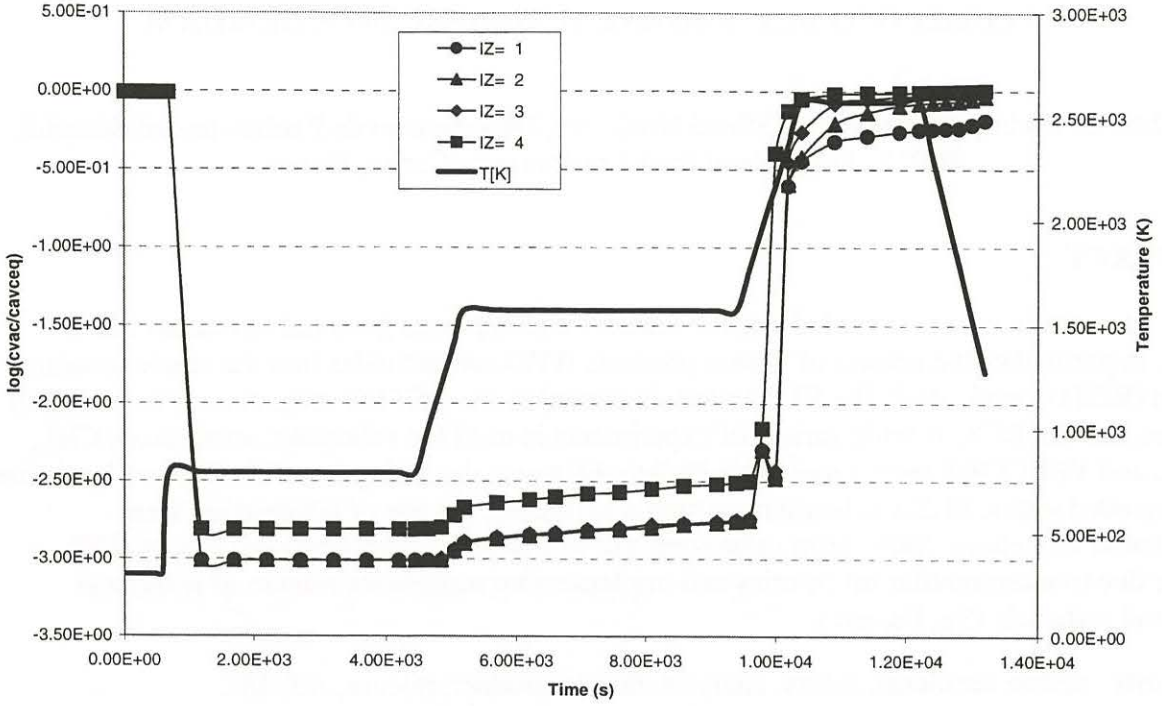

Figure 8 : Evolution of the vacancy concentration in VERCORS 4 calculated by MFPR (1.3.1). This concentration is expressed relatively to the thermal equilibrium value and given for each radial mesh of the grain.